J. Fluid Mech. (1980), *vol.* 96, *part* 4, *pp.* 757–767
Printed in Great Britain

Valley ventilation by cross winds

By ROBERT C. BELL AND RORY O. R. Y. THOMPSON†
C.S.I.R.O. Division of Atmospheric Physics, P.O. Box 77, Mordialloc, Victoria, Australia 3195

(Received 12 January 1979 and in revised form 4 April 1979)

An initial thermal stratification may be swept out of a valley if a cross-wind is strong enough: the valley is then said to be ventilated. Numerical and laboratory experiments indicate that the critical parameter is the Froude number, $F = \bar{u}/Nh$, where $\bar{u}$ is the mean horizontal velocity above the crest of the valley sides, N is the Brunt–Väisälä or bouyancy frequency of the thermal stratification in the valley air and h is the height of the valley walls. Ventilation occurs whenever the Froude number exceeds a value of 1·3.

1. Introduction

Under conditions of strongly stable thermal stratification and light winds, air can be trapped in a valley, with implications for both local weather and health. One of the authors (R. T.) was in the Willamette Valley, Oregon, U.S.A. in November 1969 when a dense fog formed and stayed for 9 days (Green 1970). Within the fog, it was unpleasantly dark, wet and cold: so cold that thick rime formed on exposed objects. Furthermore, it stank from the sulphur emissions from a paper mill in the valley. Yet at a height of about 100 m above the valley floor, the air was clean with the sun and stars shining from perfectly clear skies.

A similar event was experienced by the same author for a week in February 1976 in Bergen, Norway: from the sides of the valley above the city, distant mountains were seen under bright sunlight, but the city, only a mile away, was obscured by the thickest, brownest vehicle smog the author had ever had the misfortune to experience.

In October 1948, a smog persisted for a week in the industrial areas of the Monongahela Valley, Pennsylvania, U.S.A., causing illness to 42 % of the population and some deaths (Ashe 1952). Normally, the meteorological conditions in the 120 m deep valley are such that the air is well cleaned during the day but stagnates at night, but on this occasion the valley was not ventilated for a week resulting in a disaster to the health of many people.

Upon considering other climate effects as well, such as the frost damage to fruit crops in valleys through lack of ventilation (Geiger 1965, p. 394), it can be seen that ventilation of a valley, or its lack, is an important meteorological subject.

Previously Kaps (1955) attempted to quantify the degree of ventilation in a valley in terms of the valley geometry, but omitted the important factors of thermal stratification and ambient wind speed. Yoshino (1957) observed the winds across several valleys, finding both stagnant and sweeping flows. He fitted to the data an equation for the wind speed as a function of the distance down the slope, without taking into

† Present address: C.S.I.R.O. Division of Fisheries and Oceanography, P.O. Box 21, Cronulla, N.S.W., Australia 2230.

0022-1120/80/4369-8150 $02.00

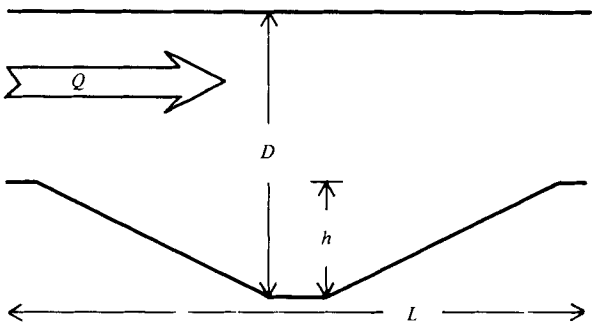

FIGURE 1. Valley shape for the numerical model. Only one wavelength (L) was used.

account the stability. Cox (1977) found observationally that emissions from a chimney in a valley could reach ground level outside the valley, whereas emissions from a similar chimney on a plain might not reach the ground, and thus a chimney in a valley is effectively shorter than one on a plain. If the emissions are in a recirculation region, they would be trapped in the valley, but even if the chimney reached above the recirculation, the emissions may reach ground level on the valley sides. However, no physical criteria were given for separating the various possibilities.

Tang (1976) considered a linear analytical model of the interaction between a large-scale flow across a valley and the thermal stratification, but with specified temperatures at the ground. A region of reversed flow was found on the upstream slope in day-time conditions and on the downstream slope in night-time conditions. Kitabayashi (1977) studied the region of stagnant flow upstream of a ridge in the atmosphere and in a wind tunnel. He concluded that stagnant flow occurs when a Froude number is less than 2·3. This value differs from the value of 1·3 found in this paper, perhaps because of the different shaped topography, different upper and side boundary conditions and different definition of the velocity scale used in the Froude number.

In this paper, a simple two-dimensional model is investigated to find out when a cross-valley wind will sweep out an initial thermal stratification. Our primary interest is in strongly stratified flows, where the effects of turbulence are small. Figure 1 shows a general view of the geometry. The key assumption is that the topography and the flow are periodic in the horizontal (x) direction with wavelength L. This obviates the major difficulty of specifying the inflow conditions in the presence of upstream influence (Baines 1977). The top of the model can be taken as representing an inversion which acts as a barrier between the flow of interest and the flow above it.

In the numerical experiments, only one period of the topography is used and the equations are simplified by making the Boussinesq, incompressible and inviscid assumptions. In the laboratory experiments, a symmetric sawtooth shaped obstacle consisting of six crests and five troughs was towed through a tank, with measurements being made above the centre of the obstacle, where the flow is close to periodic.

2. The numerical models

The dependent variables for the numerical models are the horizontal and vertical velocity components u and w, p, the perturbation pressure divided by a reference density, and the perturbation potential temperature, T. The equations used in the numerical integration are

$$u_t + \mathbf{u}.\nabla u = -p_x, \tag{1}$$

$$T_t + \mathbf{u}.\nabla T + w\Gamma = 0, \tag{2}$$

$$\nabla.\mathbf{u} = 0, \tag{3}$$

$$w_t + \mathbf{u}.\nabla w = -p_z + g\alpha T, \tag{4a}$$

$$0 = -p_z + g\alpha T, \tag{4b}$$

where t is time, Γ is the basic potential temperature lapse rate, g is gravitational acceleration and α is the coefficient of thermal expansion. Equation (4a) is the full equation for the vertical velocity component, while equation (4b) is derived from it by making the hydrostatic assumption.

The numerical models employ finite differences on a staggered grid. To simplify the computations, the lower boundary is forced to pass through grid points and to have a slope of 0 or $\pm \Delta z/\Delta x$, where Δz and Δx are the vertical and horizontal grid intervals respectively. For most of the computations, the second upwind flux form of the differences was used with the primitive equations (Roache 1972, p. 73). In this case the hydrostatic equation, (4b), was used. Equations (1) and (2) were used as prediction equations and (3) and (4b) as diagnostic equations for w and p. Mahrer & Pielke (1978) have shown that upstream differencing is quite accurate for mesoscale problems similar to the valley situation considered here. For some of the runs, the full equation for the vertical velocity component, (4a), was used, i.e. the hydrostatic approximation was not made. In this case, a stream function and vorticity formulation was integrated using the Arakawa (1966) Jacobian, but retaining the upwind flux form for the potential temperature equation. Equation (2) and the vorticity equation derived from (1) and (4a) were used as prediction equations, and a Poisson equation was solved to obtain the stream function and hence u and w from the vorticity. Figure 1 shows the lower boundary for a typical run. Basically, it is a sawtooth shape, but points on the crests and troughs have been removed to avoid strong excitation of the higher wavenumber components which might have caused trouble with the finite differences. For a typical run with total height D (the distance from the bottom of the valley to the top of the model) of 1250 m, hill height h of 500 m and length L of 4 km, a grid of 20 horizontal and 21 vertical points was used, with $\Delta x = 200$ m and $\Delta z = 62{\cdot}5$ m.

The top of the model is assumed to be a free slip rigid lid, so that the vertical velocity and heat flux are both zero there. At the lower boundary, the heat flux is zero, and near the boundary provision is made to include a heat source or sink, which in this series of experiments is taken as zero. The free slip condition $w(x, h(x)) = u(x, h(x))\, dh(x)/dx$ is used at the surface; $h(x)$ is the height of the valley wall above the level of the valley bottom ($0 \leqslant h(x) \leqslant h$). This is a reasonable condition if the lower boundary is considered to lie at some distance above the actual ground outside a thin boundary layer where viscosity is important. The free slip assumption is strengthened by the imposition of stable thermal stratification conditions under which the surface drag is

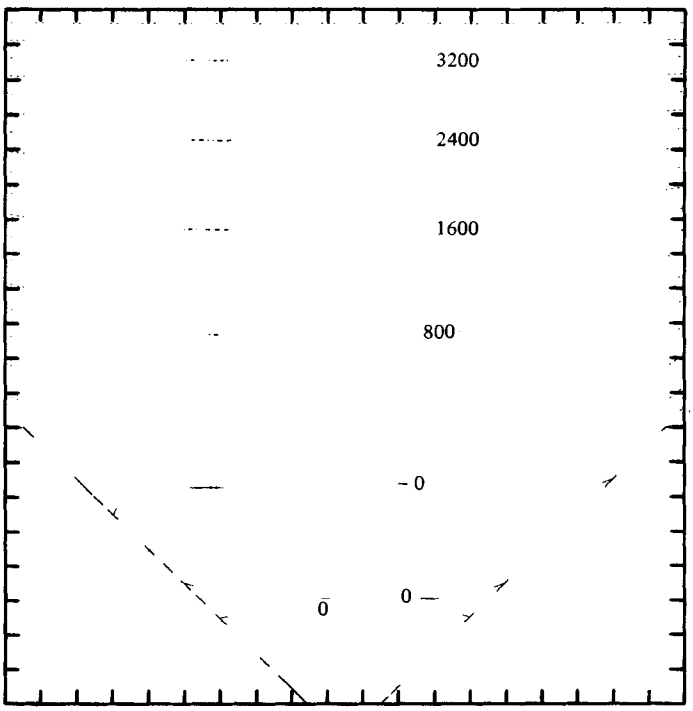

FIGURE 2. Numerical model with upwind differencing. Streamlines at 4 h for a typical stagnation case with $D/h = 2{\cdot}5$ and $F = 0{\cdot}856$. Vertical exaggeration for this figure and figures 3 and 4 is 3·2:1.

expected to be very low anyway. Apart from the artificial viscosity inherent in the finite differences, no friction is included in these integrations. Initially, a linear thermal stratification is prescribed, and the horizontal velocity component is taken to be independent of depth, i.e. $u(x) = Q/(D-h(x))$, where Q is the prescribed constant volume flux. The implementation of the periodic lateral boundary conditions is straightforward. For the upwind hydrostatic model, one other continuity condition is needed to close the system; this is constant volume flux across any vertical section. This condition corrects the instability problems Thyer (1966) had with his second model, and in many respects the present hydrostatic model is similar to it. At each time step, the horizontal velocity component u is predicted and then adjusted by a constant amount for each vertical column so that the horizontal volume flux is still the constant Q. In this way the continuity condition is satisfied. The adjustment is necessary and valid because the hydrostatic equation for the pressure specifies only the vertical pressure gradient. Using an arbitrary pressure datum for each column and integrating the diagnostic equation means that there is an error in the horizontal pressure gradient, which is constant for each column, and a similar error in the predicted horizontal velocity component. The velocity error is corrected by the procedure given above. For the Arakawa non-hydrostatic model, the continuity equation is automatically satisfied because of the stream function formulation of vorticity.

For the time stepping, the third-order predictor–corrector scheme of Thompson (1979) is used. A timestep of 5 s was found to be stable for integrations with maximum

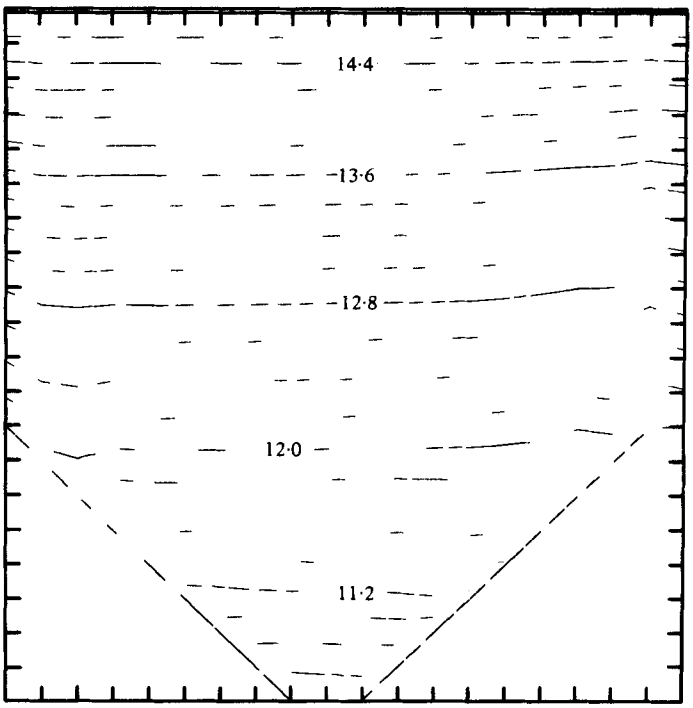

FIGURE 3. Numerical model with upwind differencing. Contours of potential temperature at 4 h for a stagnation case with $D/h = 2{\cdot}5$ and $F = 0{\cdot}856$.

velocities below about 10 m s^{-1}, but when higher velocities occurred, a 2·5 s step was necessary.

3. Results from the numerical model

The main result sought from the numerical experiments is the condition under which stagnant flow can exist in the steady state. The term stagnant flow is used here to cover both true stagnant flow where the velocity is near zero, and any situation where the streamline on the crest becomes separated at some point on the valley wall so that there is a closed circulation cell near the valley floor. The term sweeping is used to describe flows with no stagnant or reversed regions. Two parameters of the flow were varied. The first, D/h is the ratio of the total depth to the crest to trough depth of the valley, and was varied from 1·375 to 10. The second is the Froude number $F = \bar{u}/Nh$, where $\bar{u} = Q/(D-h)$ is the mean velocity over the crest, Q being the constant volume flux, N is the Brunt–Väisälä frequency for the basic stratification and h is the crest to trough depth. In the experiments, F was varied from 0·26 to infinity (corresponding to no stratification).

The aspect ratio D/L was varied in some runs, but for the hydrostatic model a simple rescaling of the results brought them back into coincidence. Specifically, if two integrations are carried out with horizontal length scales L and X, with all other parameters the same except those that depend on L (such as the grid length), then at times t and tX/L and positions (x, z) and $(xX/L, z)$ respectively, the solutions are

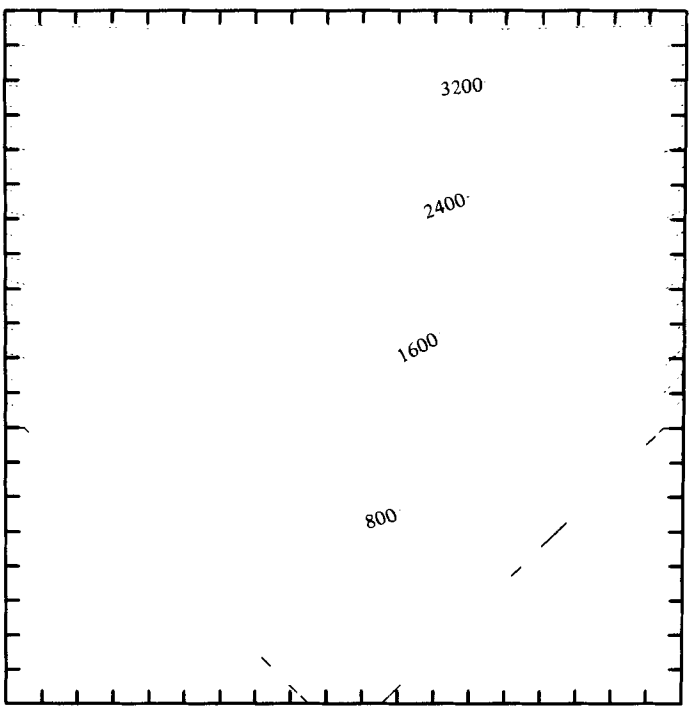

FIGURE 4. Numerical model with upwind differencing. Streamlines at 1 h for a typical sweeping flow with $D/h = 2{\cdot}5$ and $F = 1{\cdot}712$.

found to be (u, w, T, p) and $(u, wL/X, T, p)$ respectively. This scaling shows that the valley width does not alter the results; it is the vertical length scales that matter. This argument applies only to the hydrostatic model, so that the results are only independent of the horizontal length scale when the hydrostatic approximation is valid. If equation (4*a*) is non-dimensionalized using scales L, h, $\bar{u}$, and Γ, then it is found that the non-hydrostatic terms are of order $(Fh/L)^2$ of the hydrostatic terms. Almost all of the integrations of the hydrostatic upstream-differenced model have $(Fh/L)^2 < 0{\cdot}1$, with the parameter exceeding 0·1 only for large values of F with small values of D/h. Thus the hydrostatic assumption is valid for all but a few runs of this model. With the non-hydrostatic model, some integrations were carried out with the horizontal length scale halved, with values of $(Fh/L)^2$ up to 0·15; little difference was observed compared with the integrations with the larger horizontal length scale, except when D/h was small. In the atmosphere under stable conditions, F is usually $O(1)$ or less, and h/L in valleys is almost always less than, say, 0·3, so that $(Fh/L)^2 < 0{\cdot}1$, and thus the hydrostatic assumption is valid.

Most of the model integrations were extended to 1 h model time, except for a few sample and critical cases which were run up to 4 h. By 1 h, a quasi-steady state was usually reached, and the result could then be put confidently into one of the categories of stagnation or sweeping. The 1 h cut off is reasonable in view of the longest time scale in the model, namely the advection scale LD/Q which is less than 22 min for all experiments.

Figure 2 shows the streamlines for a typical stagnation case with $D/h = 2{\cdot}5$ and

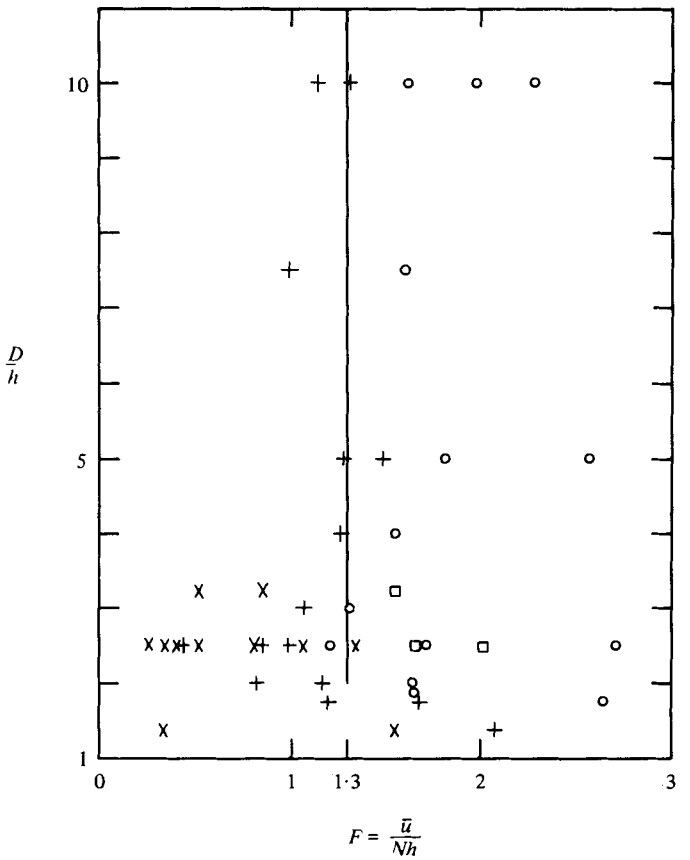

FIGURE 5. Breakdown of numerical results into sweeping or stagnant flows as a function of D/h and F. Upwind scheme: +, stagnant; (, sweeping. Arakawa scheme: ×, stagnant; □, sweeping. Note that the ordinate starts at $D/h = 1$.

$F = 0{\cdot}856$ for the upstream hydrostatic model. There is a large area in the valley where there is almost no flow, the velocities being less than $0{\cdot}5\ \mathrm{m\,s^{-1}}$ compared with $3{-}6\ \mathrm{m\,s^{-1}}$ outside. In this case, the horizontal velocity component above the crest increases slowly with height, but in other cases the situation is reversed with a marked jet over the ridge with lower velocities above. From an initial state with no stagnation, the stagnation region first appears at a time of 5 min, and grows rapidly so that at 20 min its depth is 90 % of its depth at 1 h. In general, the depth of the stagnant region at steady state increases as F is decreased from run to run. Figure 3 shows the isotherms of potential temperature for this same case. The initial potential temperature stratification is largely unchanged, so that stagnation occurs here without any marked inversion of actual temperature at the top of the stagnant region.

The streamlines for a typical sweeping flow are shown in figure 4, with $D/h = 2{\cdot}5$ and $F = 1{\cdot}712$ for the upstream hydrostatic model. The flow pattern is very similar to a potential flow for a homogeneous fluid. The isotherms of potential temperature (not shown) show a similar pattern to the stream function, as would be expected.

When D/h is small, no sweeping flows could be produced by the hydrostatic model,

even for infinite Froude number. In these cases, there is usually a very strong temperature gradient at the top of the stagnant region, with weaker gradients below. For the non-hydrostatic model, the results for small D/h depend on the horizontal length scale, with the flows tending toward stagnation as the length scale is decreased.

The results of the numerical experiments are summarized in figure 5, which shows all runs on a D/h *vs.* F diagram. Note that the ordinate D/h starts at 1·0, since $D > h$. The results were divided into the two categories of 'stagnant' if there existed a separated flow region after 1 h, and 'sweeping' if there did not. In cases near the critical line, the flow takes longer to settle down to a state in which it can be put definitely into one or the other of the categories. In some of these cases the decision was based on the flow at a time greater than 1 h, and in all these cases there is some uncertainty in the classification. It can be seen from the diagram that there is reasonably good agreement between the results of the two models.

For D/h greater than about 1·8, the critical F value can be approximated by a constant of 1·3. Stagnant flow occurs when F is less than this critical value, and sweeping flow when F exceeds this value, for both the upwind and Arakawa formulations of the model. This general behaviour could be expected from the form of F. Low values of F imply that the mean velocity is relatively slow and the thermal stratification is relatively strong, so that there is insufficient kinetic energy in the flow to lift the dense fluid near the valley floor over the crest, and stagnation results. In contrast, high F values imply that there is sufficient kinetic energy to sweep the denser fluid in the valley over the crest.

For D/h less than about 1·8, stagnation flows predominate, but the results depend on the horizontal length scale. With small values of D/h such as this, the top of the model region is close to the crest level, and the flow is forced through a narrow gap over the crest. The numerical results may be less realistic in this situation because of the greater numerical diffusion present, and because the hydrostatic approximation used with the upstream model becomes less tenable here. However, the general result of stagnation can be expected since the flow over the crest acts like a jet and continues across the valley with little expansion, and the valley is too deep for the denser fluid to be lifted over the crest. Low values of D/h are not expected to be relevant to the real atmosphere since even if an inversion could be found so close to the crest level, it would not behave as a rigid lid.

Kitabayashi (1977) also found that the critical Froude number for flow over a single step was approximately constant for values of D/h between 4 and 12·5. Thus the critical Froude number for moderate to large D/h does not depend on either D, the total depth, nor on L, the horizontal length scale.

For some runs, the initial horizontal velocity component was taken as $u = \bar{u}$ above the crest level, and zero elsewhere, corresponding to an initially stagnant state rather than a sweeping state. The stagnant initial state is in fact a steady-state solution of the equations and boundary conditions, but is an unstable state, being subject to the Kelvin–Helmholtz instability. When the initial state was perturbed, then the integrations were found to produce steady-state solutions similar to those produced from the sweeping initial conditions.

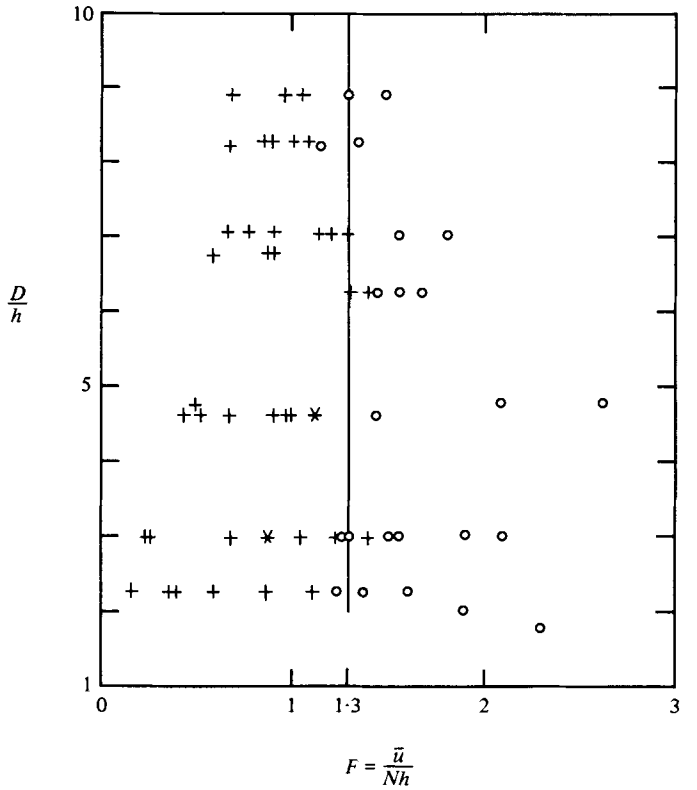

FIGURE 7. Breakdown of laboratory results into sweeping or stagnant flows as a function of D/h and F. +, stagnant; ○, sweeping; ⋇, rotor. Note that the ordinate starts at $D/h = 1$.

4. Results from laboratory experiments

The laboratory experiments were undertaken to substantiate the numerical solutions. The tank dimensions and other details are the same as Baines (1977). The tank was filled with a linearly stratified salt solution with a free surface. The towed sawtooth shape consisted of six crests and five troughs. The crests were 4 cm high and 40 cm apart.

In the early runs, the density profiles were determined by a refractometer. In later runs, an automated probe was used and provided a much more convenient check on the linearity of the density profiles. The Froude number was based on the actual density difference between 1·5 and 6 cm above the bottom, and the mean velocity $\bar{u}$ over the crest given by $\bar{u} = UD/(D-h)$, where U is the towing speed.

Figure 6 (plate 1) shows a typical flow with a stagnation region for $D/h = 8{\cdot}2$, and $F = 0{\cdot}79$. It is quite similar to figure 2 for the numerical model, after allowing for the different scale for x and z in figure 2. Sweeping flows occurred for higher Froude numbers.

The laboratory experiments produced a few flows containing a rotor, i.e. with fairly strong reverse flow near the valley floor, and with the streamlines concave up above the crests. The rotors occurred close to the values predicted by a simple linear theory of waves in a stratified fluid. Turner (1973) gives the relation

$$\omega = Nk/(k^2+m^2)^{\frac{1}{2}} \tag{5}$$

for the frequency ω of an internal wave with wavenumber (k, m) for a linear density gradient in the Boussinesq approximation. For wave resonance to occur in a bounded domain, $mD = j\pi$, $j = 1, 2\ldots$, and $\omega = k\bar{u}$, which together with (5), $k = 2\pi/L$ and the definition of F gives

$$F = DL/\pi h(4D^2+j^2L^2)^{\frac{1}{2}}. \tag{6}$$

Rotors were observed in the laboratory flows in two cases, when $D/h = 3$, $F = 0{\cdot}85$ and $D/h = 4{\cdot}65$, $F = 1{\cdot}12$. Equation (6) with $j = 1$ predicts values of F of 0·82 and 1·08 for these values of D/h, so that the agreement is close enough to conclude that rotors occur near the internal wave resonance. Note too that equation (6) is approximately $F = D/(hj\pi)$, i.e. F is proportional to D/h, which is different from the constant F behaviour of the critical line separating stagnant and sweeping flows. Rotors did occur in the numerical experiments, but were not as pronounced as in the laboratory experiments, probably because the implicit diffusion in the numerical integrations provided greater damping, and because of the rigid lid in the numerical experiments compared with the free surface in the laboratory experiments.

A diagram of all the experimental runs as a function of D/h and F is shown in figure 7. This compares well with the similar figure 5 for the numerical integrations. Again, the constant $F = 1{\cdot}3$ is a good approximation to the dividing line.

5. Conclusion

Sweeping occurs when the inertial forces dominate the buoyancy forces; stagnation occurs when the buoyancy forces dominate the inertial forces. The critical case occurs when these forces balance, and since the Froude number expresses the ratio of these forces, the critical case is expected to occur when the Froude number is of order unity. Both the numerical and laboratory experiments indicate that a constant Froude number of about 1·3 can be used to separate stagnant from sweeping flows over a valley, with stagnant flows occurring for values of F less than 1·3 and sweeping flows otherwise, provided that the ratio of the total depth to the crest to trough depth is greater than about 1·8. This result is independent of the slope of the valley sides and the total depth. For $D/h < 1{\cdot}8$, the flow tends to stagnate, although non-hydrostatic effects and the magnitude of the valley slope become important. Small values of D/h are not particularly relevant to the atmosphere since it is unlikely that a strong inversion acting as the rigid top of the model could be found so close to the ground so that $D/h < 1{\cdot}8$.

We thank George Scott and David Murray for assistance with the laboratory work and Ian Helmond for the use of his density probe.

REFERENCES

Arakawa, A. 1966 Computational design for long-term numerical integration of the equations of fluid motion: two-dimensional incompressible flow. Part 1. *J. Comput. Phys.* **1**, 119–143.

Ashe, W. F. 1952 Acute effects of air pollution in Donora, Pennsylvania. In *Air Pollution* (ed. L. C. McCabe), pp. 455–462. McGraw-Hill.

Baines, P. G. 1977 Upstream influence and Long's model in stratified flows. *J. Fluid Mech.* **82**, 147–160.

Cox, R. A. 1977 Field studies of local weather and its effects on air pollution at a proposed industrial site. *Weather* **32**, 42–56.

GEIGER, R. 1965 *The Climate Near the Ground.* Cambridge, Massachusetts: Harvard University Press.

GREEN, R. A. 1970 The weather and circulation of November, 1969. *Monthly Weather Rev.* **98**, 170–174.

KAPS, E. 1955 Zur Frage der Durchlüftung von Tälern im Mittelgebirge. *Meteorol. Runds.* **8**, 61–65.

KITABAYASHI, K. 1977 Wind tunnel and field studies of stagnant flow upstream of a ridge. *J. Met. Soc. Japan* **55**, 193–204.

MAHRER, Y. & PIELKE, R. A. 1978 A test of an upstream spline interpolation technique for the advective terms in a numerical mesoscale model. *Monthly Weather Rev.* **106**, 818–830.

ROACHE, P. J. 1972 *Computational Fluid Dynamics.* Albuquerque, New Mexico: Hermosa.

TANG, W. 1976 Theoretical study of cross-valley wind circulation. *Arch. Met. Geophys. Bioklim.* A **25**, 1–18.

THOMPSON, R. O. R. Y. 1979 A stable third-order time-integration method with minimal storage. Submitted to *Monthly Weather Rev.*

THYER, N. H. 1966 A theoretical explanation of mountain and valley winds by a numerical model. *Arch. Met. Geophys Bioklim.* A **15**, 318–348.

TURNER, J. S. 1973 *Buoyancy Effects in Fluids.* Cambridge University Press.

YOSHINO, M. 1957 The structure of surface winds crossing over a small valley. *J. Met. Soc. Japan* **35**, 184–195.

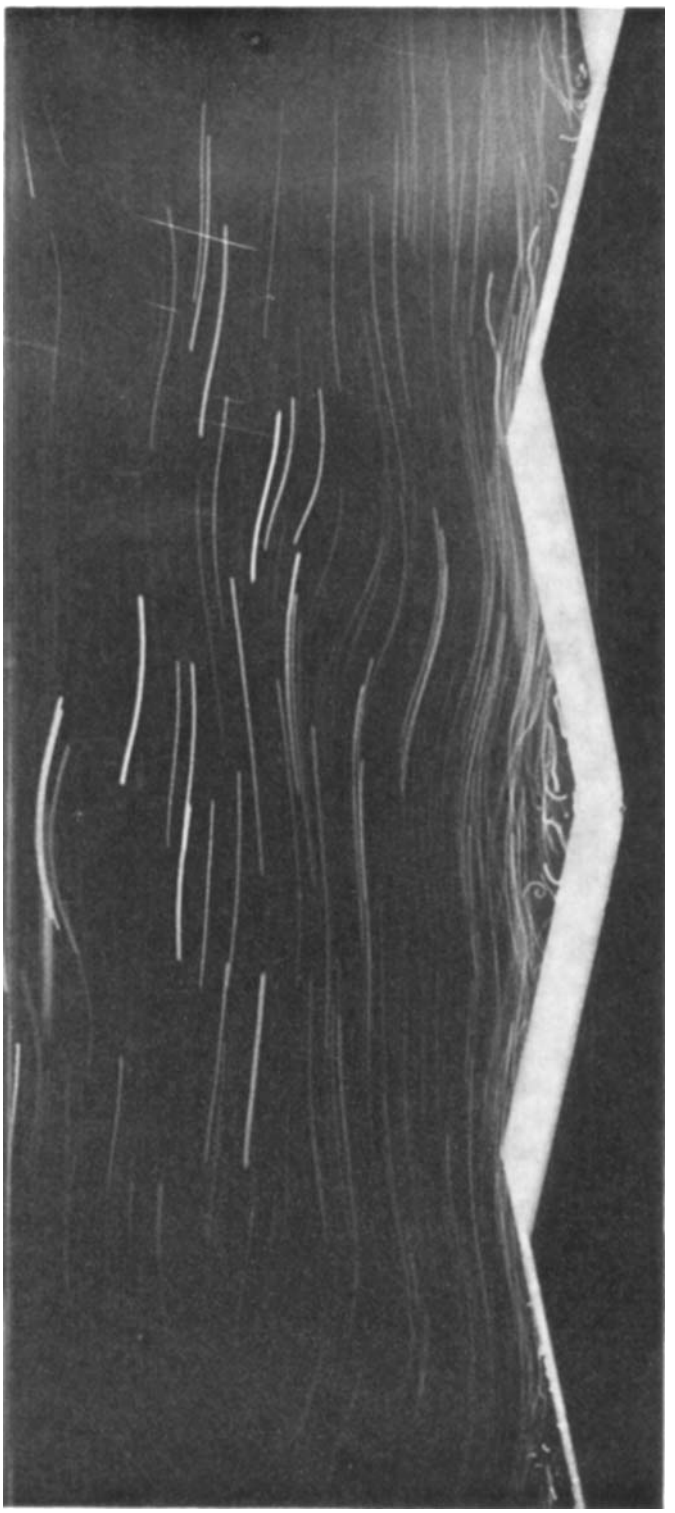

FIGURE 6. Laboratory flow for a typical stagnation case with $D/h = 8{\cdot}2$ and $F = 0{\cdot}79$.